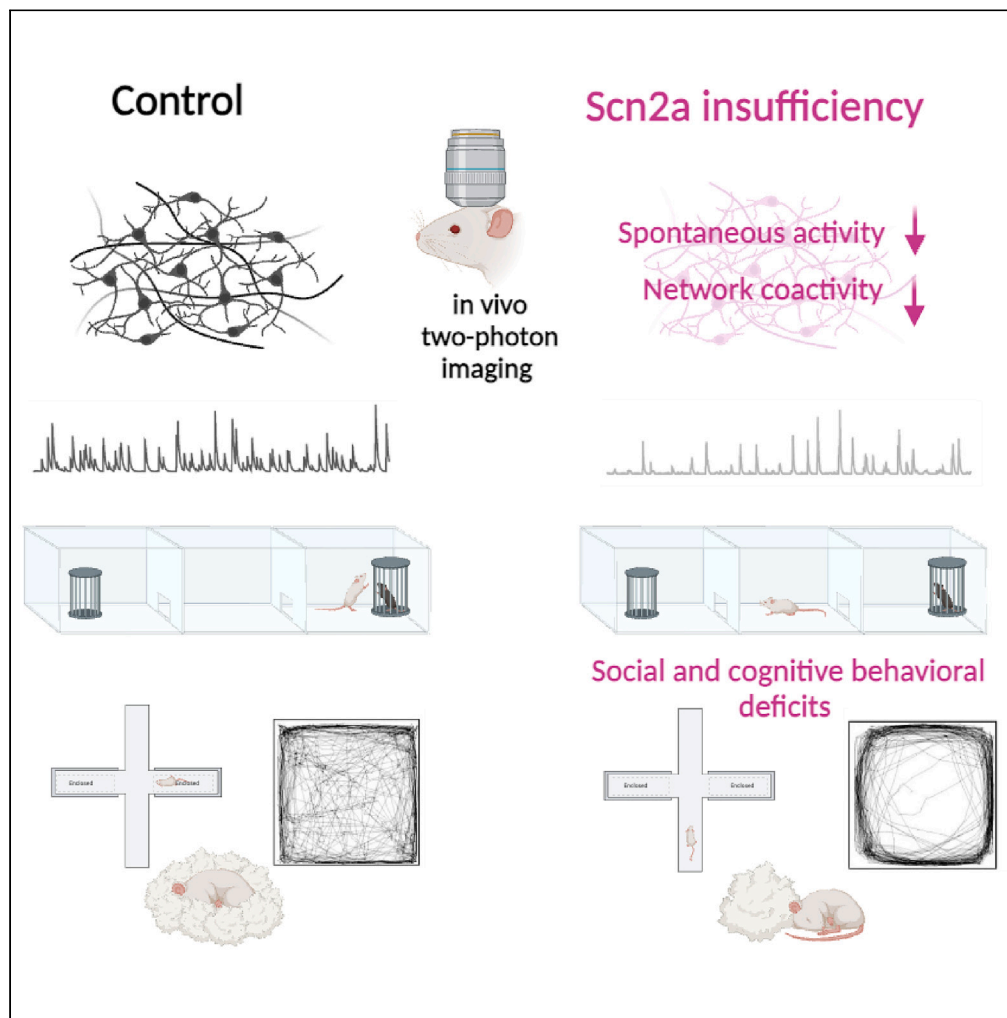


Article

Scn2a insufficiency alters spontaneous neuronal Ca^{2+} activity in somatosensory cortex during wakefulness



Melody Li,
Mohamed
Eltabbal, Hoang-
Dai Tran, Bernd
Kuhn

melody.li@florey.edu.au (M.L.)
bkuhn@oist.jp (B.K.)

Highlights

Scn2a insufficient mice showed behavioral deficits mirroring SCN2A disorders

Spontaneous cortical neuronal activities were reduced by Scn2a insufficiency

Neuronal pairwise co-activity was also decreased by Scn2a insufficiency

Li et al., iScience 26, 108138
November 17, 2023 © 2023 The
Author(s).
[https://doi.org/10.1016/
j.isci.2023.108138](https://doi.org/10.1016/j.isci.2023.108138)



Article

Scn2a insufficiency alters spontaneous neuronal Ca^{2+} activity in somatosensory cortex during wakefulnessMelody Li,^{1,*} Mohamed Eltabbal,¹ Hoang-Dai Tran,¹ and Bernd Kuhn^{1,2,*}

SUMMARY

SCN2A protein-truncating variants (PTV) can result in neurological disorders such as autism spectrum disorder and intellectual disability, but they are less likely to cause epilepsy in comparison to missense variants. While *in vitro* studies showed PTV reduce action potential firing, consequences at *in vivo* network level remain elusive. Here, we generated a mouse model of Scn2a insufficiency using antisense oligonucleotides (Scn2a ASO mice), which recapitulated key clinical feature of SCN2A PTV disorders. Simultaneous two-photon Ca^{2+} imaging and electrocorticography (ECoG) in awake mice showed that spontaneous Ca^{2+} transients in somatosensory cortical neurons, as well as their pairwise co-activities were generally decreased in Scn2a ASO mice during spontaneous awake state and induced seizure state. The reduction of neuronal activities and paired co-activity are mechanisms associated with motor, social and cognitive deficits observed in our mouse model of severe Scn2a insufficiency, indicating these are likely mechanisms driving SCN2A PTV pathology.

INTRODUCTION

The SCN2A gene encodes the alpha subunit of the voltage gated sodium channel (VGSC) Nav1.2. Scn2a is highly expressed in excitatory neurons,¹ and can be detected in somata, dendrites, axon initial segments, and unmyelinated axons.^{2–4} An activated Nav1.2 conducts an inward current of sodium ions, subsequently depolarizing the neuronal membrane.⁵ During early brain development, Nav1.2 has been shown to be critical for action potential (AP) initiation and propagation in neocortical pyramidal neurons, when it is the predominant VGSC.^{6–8} Later in life, the role of Nav1.2 in AP initiation is largely replaced by another VGSC, Nav1.6. However, Nav1.2 remains crucial for somato-dendritic signaling.²

Genetic variations in SCN2A can result in a range of neurodevelopmental disorders and the phenotypic spectrum continues to expand.^{9–12} Pathological SCN2A variants can be grouped by clinical presentation such as age of disease onset.^{9–11} They can also be grouped into gain-of-function (GoF) or loss-of-function (LoF) based on their effect on the channel's biophysical properties as determined in heterologous expression systems.^{13–15} It is hypothesized that GoF variants, which consist of missense variants, are associated with early-onset epilepsies.^{9,11,14,15} In contrast, LoF variants can be missense, deleterious, and protein truncating and they are associated with late-onset epilepsies and non-epilepsy phenotypes such as autism spectrum disorder (ASD) and intellectual disability (ID).^{14,15} Specifically, patients with protein-truncating variants (PTV) are less likely to have epilepsy than individuals with missense (GoF and LoF) variants.¹² Recently, patient-derived neurons which expressed a stop variant were found to mediate smaller current and fire less AP than isogenic controls.¹⁶ However, the consequences of these *in vitro* cellular changes on brain network remains unclear.

Mouse models of Scn2a insufficiency can be viewed as proxy models for Scn2a PTV disorders and enables the examination of functional consequences of reduced Scn2a function at behavioral, network, and cellular levels. The use of Scn2a insufficient mice was complicated by the observation that Scn2a homozygous knockout (KO) mice die perinatally,¹⁷ while heterozygous KO mice showed subtle behavioral phenotypes that do not entirely reflect the clinical severity of SCN2A PTV disorders.^{2,18–20} Recently two different mouse models of Scn2a insufficiency were generated using gene trap technology²¹ and virus transduction.²² Robust behavioral and cellular changes were reported in these mice whereby Scn2a expression was reduced to 10–25%.^{21–23} Whole cell recordings in brain slices found elevated somatic AP firing in both Scn2a insufficient mouse models across different excitatory neuronal types.^{21,22} On the other hand, backpropagating action potentials (bAP) were severely impaired by Scn2a insufficiency.^{21,22} bAP act as a feedback signal, reporting somatic output activities back to dendrites, and are well known to modulate synaptic efficacy and dendritic integration.^{24–27} It is unclear how two seemingly opposite changes in single neuron excitability (increased somatic AP firing and decreased bAP) affect neuronal population activities.

¹Optical Neuroimaging Unit, Okinawa Institute of Science and Technology Graduate University (OIST), 1919-1 Tancha, Onna-son, Okinawa 904-0495, Japan

²Lead contact

*Correspondence: melody.li@floreys.edu.au (M.L.), bkuhn@oist.jp (B.K.)
<https://doi.org/10.1016/j.isci.2023.108138>



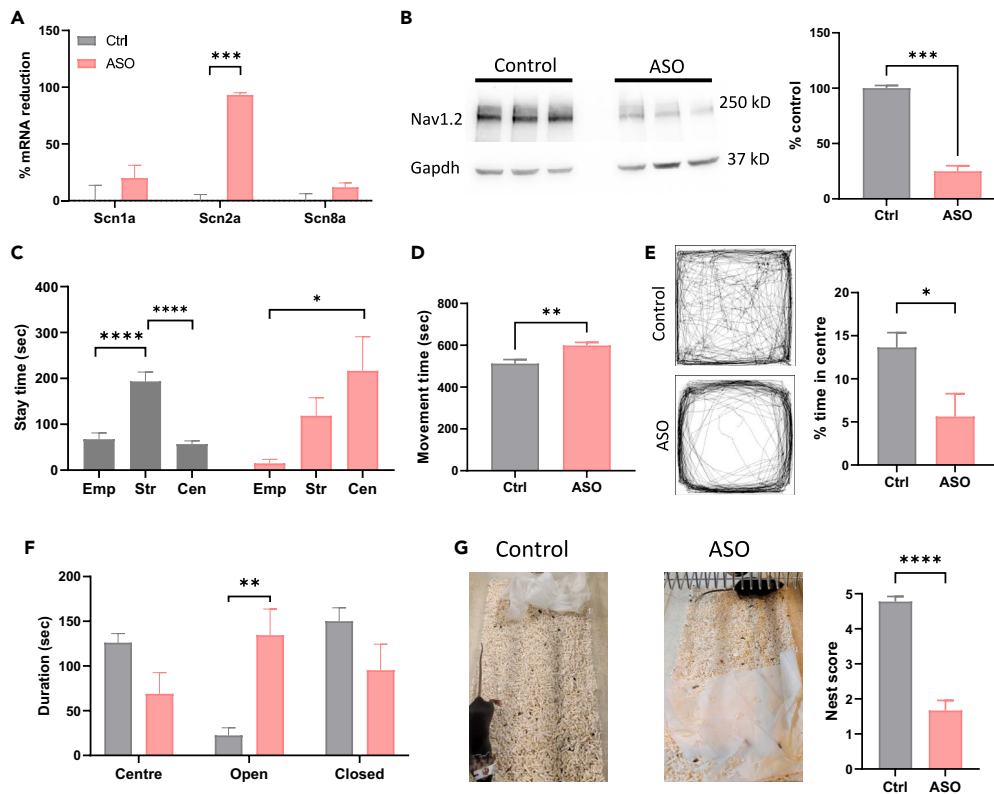


Figure 1. Characterization of the Scn2a ASO mouse model

(A) Scn1a, Scn2a, and Scn8a mRNA expression in mice ICV injected with control (PBS) or Scn2a ASO (500 μ g). N = 3 for both groups. ***p = 0.001, unpaired t-test. (B) Nav1.2 protein levels measured from whole brain lysates. N = 3 for both groups. ***p = 0.0002, unpaired t-test. (C) Time spent in the different compartments of the three-chamber social interaction test: empty (Emp), stranger (Str), and center (Cen). ****p < 0.0001, *p < 0.05, one-way ANOVA with Tukey's multiple comparison. (D) Movement duration in open field. **p < 0.01, unpaired t-test. (E) Representative movement traces in open field and the percentage time spent in the center or outer region of the open field. *p < 0.05, unpaired t-test. (F) Duration on the different sections of elevated plus maze. **p < 0.01, two-way ANOVA with Sidak's multiple comparison. (G) Representative nest photos and the nest score determined 48 h after nesting material was given. Control N = 8–9 mice and Scn2a ASO N = 9–10 mice for all behavioral tests. All data presented as mean \pm sem.

In this study, we applied two-photon *in vivo* Ca²⁺ imaging to measure activities of a population of cortical excitatory neurons in a mouse model of Scn2a insufficiency. This technique is well established and enabled us to measure from awake mice and in a condition where most neuronal processes are not severed. Additionally, electrocorticography (ECoG) was recorded simultaneously with Ca²⁺ imaging to monitor whole brain activity. Since atypical sensory processing is one of the characteristics of ASD and excitation/inhibition imbalance were reported in the somatosensory cortex of several mouse models of ASD,^{28,29} this study performed functional Ca²⁺ imaging in the somatosensory cortex. Specifically cortical layer 5 (L5) neurons were selected as they were impacted by Scn2a insufficiency.²² Examining the population neuronal activities in Scn2a insufficient mice will provide further insights into the disease mechanisms driving SCN2A PTV pathology.

RESULTS

ASO-mediated Scn2a insufficient mice displayed motor, social, and cognitive deficits

The Scn2a insufficient mouse model used in this study was created by injecting an established antisense oligonucleotides (Scn2a ASO, 500 μ g) that selectively downregulate mouse Scn2a mRNA and protein expression into the ventricles of adult mice (2–3 months old).³⁰ This delivery method is known to achieve widespread ASO distribution and ASO-mediated Scn2a knockdown in all brain regions.^{30–32} The effect of ASO is not known to be brain region dependent.³² The efficacy and selectivity of the Scn2a ASO was validated by qPCR, where we observed 93.21 \pm 3.51% reduction in Scn2a mRNA expression in comparison to control (PBS) (Figure 1A). The Scn2a ASO did not change the mRNA levels of the other two common VGSCs in the brain, Scn1a and Scn8a (Figure 1A). The effect of ASO was also seen at protein level, where Nav1.2 was reduced to 24.91 \pm 5.07% of the control group (Figure 1B). The efficacy of Scn2a ASO was previously shown to peak at 2 weeks after administration and *in vivo* half-life can be up to several months due to chemical modifications protecting ASO from nuclease-mediated digestion

and improving their pharmacokinetic properties.³³ Therefore, all behavioral and *in vivo* Ca²⁺ imaging experiments in this study were performed within 2–4 weeks after ASO injection.

A battery of behavioral tests was performed to determine if our Scn2a insufficient mice (Scn2a ASO mice) display relevant biomarkers for SCN2A PTV disorders. A prevalent PTV phenotype is ASD,^{9,12,13} so the three-chamber social interaction test was first performed. As expected, control mice spent more time interacting with the cage containing stranger mouse than the empty cage or the center compartment of the three-chamber apparatus (Figure 1C). In contrast, Scn2a ASO mice showed no preference to the stranger mouse cage and spent significantly more time in the center compartment (Figure 1C). The three-chamber test results indicated social avoidance and impaired social approach in Scn2a ASO mice.

SCN2A LoF clinical features also include movement abnormalities and hyperactivity.¹² In open field, Scn2a ASO mice displayed higher ambulatory duration (Figure 1D). Furthermore, analysis of the movement traces revealed they spent significantly less time in the center of the open field apparatus (Figure 1E), suggesting thigmotactic behavior. Previous studies in other Scn2a insufficient mouse models reported cognitive related abnormalities.^{2,19,34} Here, the Scn2a ASO mice spent more time in the open arms of the elevated plus maze (Figure 1F), which can be interpreted as the inability to assess risks. The Scn2a ASO mice also lost the instinctive rodent behavior of nest building (Figure 1G). Overall, the Scn2a ASO mice mirrored key clinical features of SCN2A PTV disorders including motor, social, and cognitive abnormalities. Thus, they can be viewed as a proxy model to infer pathological consequences caused by SCN2A PTV.

Scn2a insufficiency decreased spontaneous single neuron Ca²⁺ activities

Previous brain slice studies found that severe Scn2a insufficiency led to increased somatic AP firing but impaired bAP across different types of excitatory neurons in different brain regions.^{21,22} In this study, we would like to investigate how these changes in a single neuron manifest at a population level. To examine activities of a neuronal population with single-cell resolution, two-photon Ca²⁺ imaging was performed in awake, head-fixed mice that could move freely on a cylindrical treadmill. Additionally, ECoG was recorded simultaneously.

Since Scn2a is ubiquitously expressed in excitatory neurons and multiple brain regions are implicated in SCN2A PTV pathology, we decided to first record from cortical L5 pyramidal neurons in the S1 Cx. Previous brain slice study showed that excitability of cortical L5 pyramidal neurons were impacted by Scn2a insufficiency^{2,22} and spike wave discharges-like ECoG abnormality was observed in the somatosensory cortex of Scn2a heterozygous KO mice.^{35–37} Furthermore, altered excitation/inhibition balance was reported in established mouse models of ASD.^{28,29} Viral plasmids containing the genetically encoded Ca²⁺ indicator GCaMP6f, expressed Cre-dependent under a synapsin promoter, were locally injected into S1 Cx of Rbp4-Cre mice to selectively label L5 pyramidal neurons (Figure 2A).

In all experiments, frame scans with a field of view of 375 × 375 μm were acquired (Figure 2B). The imaging depth ranged from 520 to 580 μm from dura. On average, 73 ± 7 and 74 ± 6 active somata were recorded for control (N = 6 mice) and Scn2a ASO mice (N = 7 mice), respectively. Ca²⁺ transients as indicated by relative fluorescence change (ΔF/F) were extracted from a total of 438 regions of interest (ROIs) from control mice and 515 ROIs from Scn2a ASO mice. Signals which passed 2.5 above standard deviation of baseline fluctuations were classified as Ca²⁺ transients (Figure 2C). Spontaneous activity of L5 soma was recorded for 30 min. Animals were then injected with the pro-convulsant, pentylenetetrazol (PTZ), and activities were recorded for a further 30 min (Figure 2D). Ca²⁺ events from individual neurons were pooled and quantified by their mean amplitude, frequency and normalized integral. As neuronal activities within a population are not truly independent from one another, intra-class correlation (ICC) values were first calculated and found low clustering in this *in vivo* Ca²⁺ imaging dataset (Table S1). A linear mixed effect (LME) model³⁸ was then applied to examine the three fixed effects: (1) Scn2a ASO, (2) PTZ treatment, and (3) interaction between Scn2a ASO and PTZ treatment. The statistical summary is detailed in Table S2.

ICV injection of Scn2a ASO to mice significantly increased the mean amplitude of spontaneous Ca²⁺ transients (Figure 3A). However, it significantly lowered the frequency of Ca²⁺ transients (Figure 3B), resulting in an overall dampening effect on the spontaneous Ca²⁺ activities of S1 Cx L5 pyramidal neurons, as demonstrated by significant reduction in the normalized integral estimates (Figure 3C; Table S2).

Neuronal pairwise co-activities were reduced by Scn2a insufficiency

Since single neuron activities were altered in Scn2a ASO mice, we then asked if connectivity within the neuronal population was also affected. Here connectivity between neuronal pairs was measured using cosine similarity.³⁹ A similarity index (SI) was calculated for each pair, where an SI of 0 indicates no similarity, and 1 indicates identical activity. A bootstrapping procedure,⁴⁰ which involved repeated random shuffling of individual neurons' time courses, was performed. At each shuffle step, SI was calculated for all pairs. Thus, a surrogate dataset of pairwise similarity expected at chance level was generated for each neuronal pair. The observed SI of each neuronal pair was then compared to the surrogate dataset, and significant similarity was identified when passed the 95 percentile (Figure 3D). Our analysis revealed Scn2a ASO decreased the averaged SI (Figure 3E), suggesting Scn2a insufficiency reduces the connectivity and potentially synchronicity within the S1 Cx L5 neuronal population during spontaneous activities. Altered neuronal network connectivity and synchrony may be reflected on changes in power and frequency of ECoG oscillations. However, in the simultaneous ECoG recording, power spectrum density analysis found no differences between Scn2a ASO or control mice across frequency bands (Figure S1).

Scn2a insufficiency altered response to pro-convulsant perturbation

Patients with SCN2A PTV are likely to be associated with epilepsy in comparison to other SCN2A missense variants.¹² Consistent with clinical observations, no spontaneous behavioral seizures were observed in Scn2a ASO mice and ECoG did not detect any ictal features. However,

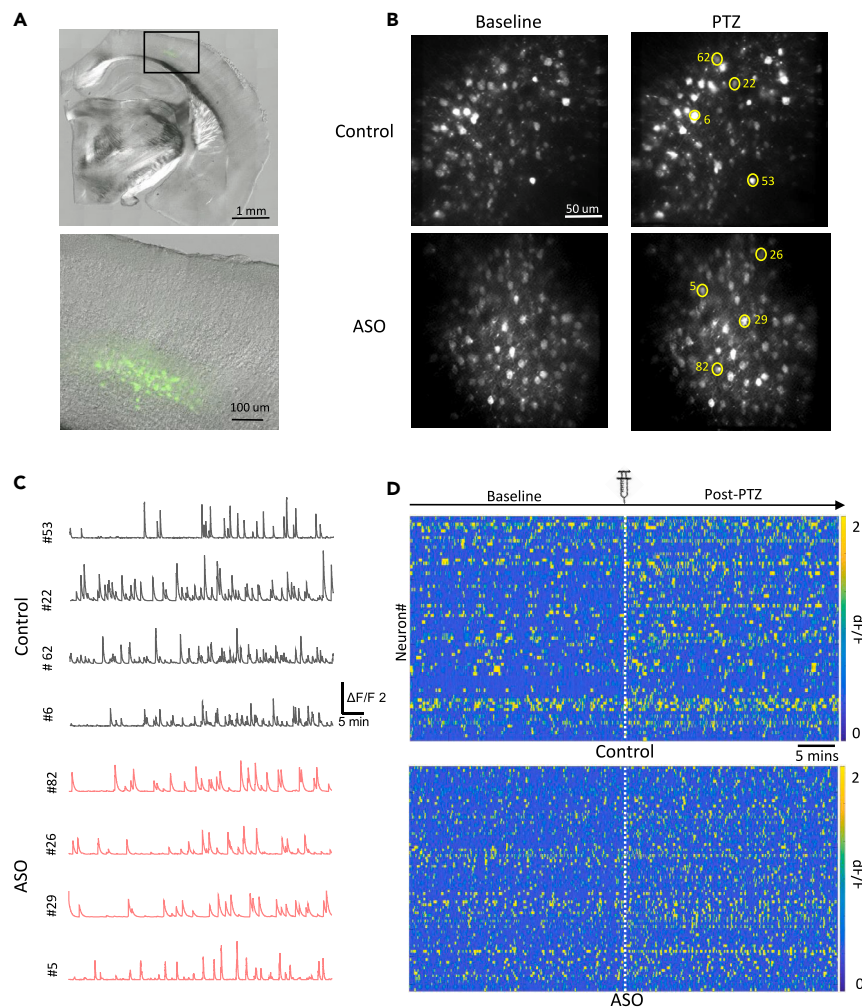


Figure 2. Two photon *in vivo* calcium imaging in somatosensory cortical L5 neurons

(A) Image of fixed brain slice showing GCaMP6f expression in somatosensory cortical L5 neurons.
 (B) Representative field of views acquired from a control and Scn2a ASO mouse during baseline and after injection of PTZ.
 (C) Representative $\Delta F/F$ extracted from cells as indicated in (B).
 (D) Representative heat maps of $\Delta F/F$ from a control (69 ROIs) and Scn2a ASO mouse (82 ROIs).

given increased somatic AP firing was reported in brain slice studies of severe Scn2a insufficient mice,^{21,22} the heightened seizure threshold may be revealed by a pro-convulsant challenge. Therefore, we injected mice with PTZ (50 mg/kg) a commonly used chemical pro-convulsant that cause seizures via GABAergic inhibition,^{41,42} and recorded neuronal activities for 30 min.

As expected, in both control and Scn2a ASO mice, Ca^{2+} transients' amplitude, frequency, normalized integral and pairwise co-activities were all increased after PTZ administration (Figures 3A–3E; Table S2). For both the mean amplitude and frequency of individual neurons' Ca^{2+} transients, the effect of Scn2a ASO was not altered by PTZ treatment, as shown by the non-significant interaction between the two fixed effects in the LME model (Figures 3A and 3B). For normalized integral, there was a significant interaction between Scn2a ASO and PTZ treatment. The Scn2a ASO mice showed an augmented response to PTZ in comparison to control mice (Figure 3C). Despite this augmented response, the normalized integral values after PTZ treatment were not different between control and Scn2a ASO mice. A significant interaction between Scn2a ASO and PTZ treatment was also determined for neuronal pairwise co-activity. Here, the Scn2a ASO mice showed reduced response to PTZ compared to control mice (Figure 3E; Table S2).

Simultaneous ECoG recordings detected PTZ induced ictal spikes in both control and Scn2a ASO mice. Though there was a trend toward lower number of spikes in Scn2a ASO mice, the difference was not statistically significant (Figure 4A). However, spectral analysis determined Scn2a ASO mice had lower delta power than control mice (Figure 4B), and the delta oscillations have been associated with decreased network synchrony⁴³ (Figure 4B). Both *in vivo* Ca^{2+} imaging and ECoG data would suggest the Scn2a ASO mice were less sensitive to PTZ induced hyper-synchrony.

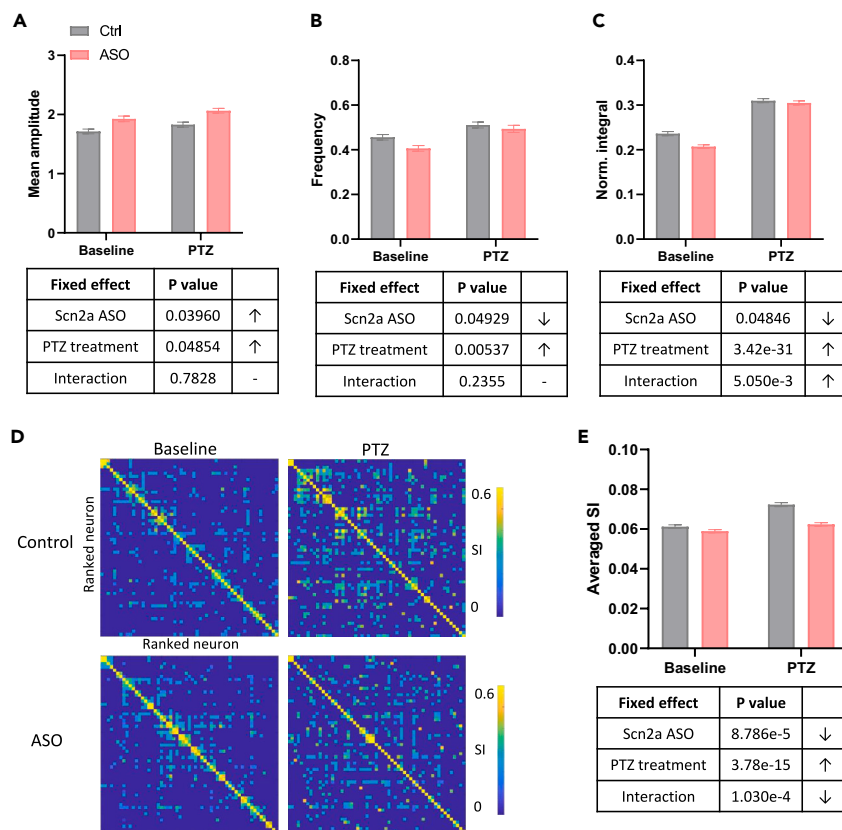


Figure 3. Altered calcium transient properties and pairwise co-activities in Scn2a ASO mice

(A–C) Calcium transient properties quantified from pooled individual neurons. (A) Mean amplitude.

(B) Frequency.

(C) Normalized integral.

(D) Representative heat maps indicating the similarity indices (SI) of all neuronal pairs from a control and Scn2a ASO mouse during baseline and after PTZ.

(E) Averaged SI of control and Scn2a ASO neuronal pairs.

Control N = 438 ROIs from 6 mice, Scn2a ASO N = 515 ROIs from 7 mice. p values were determined using linear mixed effect model, arrows indicate the direction of change based on estimate of mean (Table S2). All data presented as mean ± sem.

DISCUSSION

In this study, we established a novel mouse model of Scn2a insufficiency using ASO and identified multiple behavioral deficits that are relevant to clinical symptoms of SCN2A PTV disorders, thus positioning this mouse model as a proxy model with high face validity for SCN2A PTV disorders. This also expanded the repertoire of mouse models that can be used to infer functional consequences of SCN2A PTV. The ASO method is distinctive from other existing models in several aspects. First it enables acute but long-lasting Scn2a downregulation in any mouse strains, by-passing rounds of animal breeding. Secondly, the use of ASO also gives temporal flexibility to decrease Scn2a at any developmental stages as early as *in utero* to adulthood.^{30,44} Lastly, it is possible to neutralize the effect of ASO using antibodies, opening the possibilities to examine if altered neuronal activities persist after the molecular mechanisms have been reversed.³³

To understand the functional consequences of SCN2A PTV, previous studies used brain slice electrophysiology and identified increased somatic AP firing but impaired bAP in mouse models of severe Scn2a insufficiency,^{21,22} raising the question as to how these opposite changes in a single neuron is reflected at synaptic and neuronal population level. *In vivo* two-photon Ca²⁺ imaging can address this question with the advantage of measuring activities from a population of neurons with single neuron resolution in intact brains of awake mice.^{43,45,46} The better preservation of brain integrity would improve the physiological relevance especially when investigating changes at a network level. The higher mean amplitude of Ca²⁺ transients in Scn2a ASO mice, which indicate AP bursts,⁴⁷ is consistent with the observation made in brain slices, where neurons from severe Scn2a insufficiency display initial burst firing pattern.²² However, this burst firing did not lead to higher overall activity in Scn2a ASO mice. In fact, their Ca²⁺ transients were significantly less frequent, resulting in an overall decrease in spontaneous Ca²⁺ activities in S1 Cx L5 pyramidal neurons. The exact mechanism underlying this reduction in spontaneous activities is unclear, but it is likely that Scn2a mediated bAP plays a more critical role in modulating network activities than somatic AP. It is well established that bAP promote synaptic integration and plasticity,^{24–27} and Scn2a is one of the main contributors of bAP.¹ Therefore, severe Scn2a insufficiency may

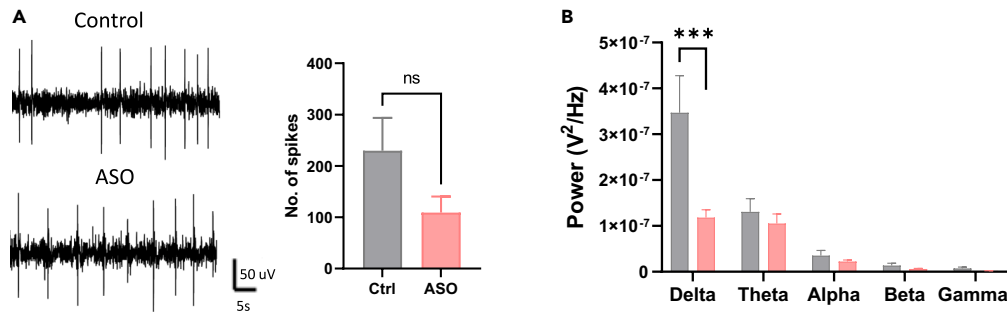


Figure 4. ECoG response to PTZ induced ictal state

(A) Representative of PTZ induced ictal spikes (left) and number of spikes recorded 30 min after PTZ administration (right). $p = 0.191$, unpaired t-test. €.
(B) Power of different frequency bands after PTZ. Delta (1–4 Hz), theta (5–8 Hz), alpha (9–14 Hz), beta (15–30 Hz), gamma (30–50 Hz). *** $p < 0.001$, across all frequency bands, two-way ANOVA with Sidak's multiple comparison. Control N = 4 mice, Scn2a ASO N = 3 mice. All data presented as mean \pm sem.

disrupt the ability a neuronal population to integrate signals. In support of this, our *in vivo* Ca²⁺ imaging found the co-activity between neuronal pairs was significantly lower in Scn2a ASO mice.

While SCN2A PTV are less likely to be associated with epileptic phenotypes, hyper-excitability were reported from brain slice studies in mouse models of severe Scn2a insufficiency,^{21,22} and spike-wave discharge like features were detected on ECoG in Scn2a heterozygous KO mice.^{36,37} Thus, this study explored potential seizure phenotypes in the Scn2a ASO mouse model. No spontaneous seizure or ictal features were observed in Scn2a ASO mice during experimental period. The GABAergic transmission inhibitor, PTZ, also did not reveal heightened susceptibility to induced seizures in Scn2a ASO mice in both *in vivo* Ca²⁺ imaging and ECoG recording. Interestingly, individual neuronal activities were more sensitive to PTZ in Scn2a ASO mice but neuronal pairwise co-activity in Scn2a ASO mice remained lower than control, reinforcing that Scn2a insufficiency may severely impair neuronal signal integration and synchronization. The lack of seizure phenotype was not limited to the Scn2a ASO mouse model but was also observed in other Scn2a insufficient mice.^{2,18–20,22,23,48}

The reduced spontaneous single neuron Ca²⁺ activity and pairwise co-activity may underlie the abnormal behaviors observed in Scn2a ASO mice, though both increased and reduced Ca²⁺ activities were reported from existing mouse models of ASD and ID.^{49–51} To better understand if the changes in Ca²⁺ activities observed in Scn2a ASO mice is directly driving the ASD or ID behavior, future *in vivo* Ca²⁺ imaging studies could include a behavioral component such as social cue presentations, cognitive tasks, or sensory stimuli and measure activities in the corresponding brain regions. This would better ascertain if the cellular changes were causal to behavioral abnormalities, as neuronal signaling during social, learning, and sensory behavior can be highly context dependent.^{52–54}

Limitations of the study

The study aimed to explore the functional consequences of Scn2a insufficiency using *in vivo* measuring methods. Here, we used an ASO that selectively reduced Scn2a by approximately 90% and observed modest behavioral and cellular changes. However, patients are heterozygous for SCN2A PTV, but previous studies showed 50% Scn2a reduction only led to subtle phenotypes in mice.^{2,18,19,48} While not ideal, more than heterozygosity is sometimes required when modeling genetic neurodevelopmental disorders in mice given the fundamental differences between human and mouse neurophysiology.^{55,56} Another caveat of the Scn2a ASO mouse model is that Scn2a expression is reduced later in life, rather than from conception. Despite later reduction in Scn2a, pronounced cognitive, social, and mild motor abnormalities were still observed here in this study. It appears in rodents, acute downregulation of Scn2a function is sufficient to cause PTV-like pathology. Therefore, caution should be taken when directly inferring disease mechanisms of SCN2A PTV from these proxy mouse models. It also highlights the need to model SCN2A PTV with different approaches such as using patients' stem cell derived neurons and brain organoids, which might offer higher resemblance to human physiology.

Since bAP were not recorded in this study, it is not possible to confirm if impaired bAP is the cellular mechanism underlying lowered Ca²⁺ activities and co-activities in the Scn2a ASO mouse model. Whole-cell recordings could be performed in future studies to study bAP in brain slices obtained from Scn2a ASO mice and compare with existing models of severe Scn2a insufficiency.^{21,22} To minimize damages to neuronal connections, an alternative approach would be to perform *in vivo* recordings or voltage imaging.^{57,58}

It remains unknown whether the reduced Ca²⁺ single neuron and paired co-activity will be observed across different cell types and brain regions. While the somatosensory cortex was implicated in ASD, in particular the altered tactile response observed in patients,^{28,29} other brain regions such as the prefrontal cortex also plays a critical role in social and cognitive function.^{59,60} Our ability to examine multiple brain regions simultaneously is limited by the field of view of the current *in vivo* Ca²⁺ imaging platform. However, future studies could build upon these existing observations and perform *in vivo* imaging in other brain regions in the Scn2a ASO mice.

Conclusions

By performing two-photon Ca²⁺ imaging in a proxy mouse model of SCN2A PTV, we provided the first observation of the effect of severe Scn2a insufficiency in S1 Cx neuronal population of awake mice. The ability to resolve single neuronal activities from intact brains of live

animals provides a novel perspective into the functional consequences of reduced *Scn2a* function, and data can be interpreted in complement to brain slice electrophysiology or other electrical measurements such as local field potentials. Our functional imaging data found reduced overall dampening of single neuron Ca^{2+} activity and pairwise coactivity during both spontaneous wakefulness and in PTZ induced ictal state, thus providing a basis to further investigate SCN2A PTV disease mechanisms.

STAR★METHODS

Detailed methods are provided in the online version of this paper and include the following:

- KEY RESOURCES TABLE
- RESOURCE AVAILABILITY
 - Lead contact
 - Materials availability
 - Data and code availability
- EXPERIMENTAL MODEL AND STUDY PARTICIPANT DETAILS
 - Animals
- METHOD DETAILS
 - Drug preparation
 - Quantitative gene expression analysis (RT-qPCR)
 - Western blotting
 - Surgery
 - Behavioral tests
 - Open field
 - Elevated plus maze
 - Nesting
 - Three-chamber social interaction test
 - Simultaneous *in vivo* Ca^{2+} imaging and electrocorticography
 - *In vivo* Ca^{2+} imaging and electrocorticography analyses
- QUANTIFICATION AND STATISTICAL ANALYSIS

SUPPLEMENTAL INFORMATION

Supplemental information can be found online at <https://doi.org/10.1016/j.isci.2023.108138>.

ACKNOWLEDGMENTS

The authors thank the OIST Animal Resources Section, Imaging Section and Kazuo Mori and Sigita Augustinaite for their help and technical support, and the OIST Graduate University for generous financial support. This work was supported by JSPS Fellowship and JSPS KAKENHI Grant (21F20712, 22J10169) awarded to M.L. and M.E respectively.

AUTHOR CONTRIBUTIONS

M. Li: conceptualization, methodology, investigation, analysis, funding acquisition, writing – original draft, review and editing. M. Eltabbal: analysis, funding acquisition, writing – review and editing. H.-D.T.: western blot, writing – review and editing. B.K.: conceptualization, methodology, supervision, writing – review and editing.

DECLARATION OF INTERESTS

The authors declare no competing interests.

Received: April 17, 2023

Revised: July 22, 2023

Accepted: October 2, 2023

Published: October 5, 2023

REFERENCES

1. Hu, W., Tian, C., Li, T., Yang, M., Hou, H., and Shu, Y. (2009). Distinct contributions of $\text{Na}(\nu)$ 1.6 and $\text{Na}(\nu)$ 1.2 in action potential initiation and backpropagation. *Nat. Neurosci.* 12, 996–1002. <https://doi.org/10.1038/nn.2359>.
2. Spratt, P.W.E., Ben-Shalom, R., Keeshen, C.M., Burke, K.J., Jr., Clarkson, R.L., Sanders, S.J., and Bender, K.J. (2019). The Autism-Associated Gene *Scn2a* Contributes to Dendritic Excitability and Synaptic Function in the Prefrontal Cortex. *Neuron* 103, 673–685.e5. <https://doi.org/10.1016/j.neuron.2019.05.037>.
3. Boiko, T., Rasband, M.N., Levinson, S.R., Caldwell, J.H., Mandel, G., Trimmer, J.S., and Matthews, G. (2001). Compact myelin

- dictates the differential targeting of two sodium channel isoforms in the same axon. *Neuron* 30, 91–104. [https://doi.org/10.1016/s0896-6273\(01\)00265-3](https://doi.org/10.1016/s0896-6273(01)00265-3).
4. Boiko, T., Van Wart, A., Caldwell, J.H., Levinson, S.R., Trimmer, J.S., and Matthews, G. (2003). Functional specialization of the axon initial segment by isoform-specific sodium channel targeting. *J. Neurosci.* 23, 2306–2313.
 5. Rush, A.M., Dib-Hajj, S.D., and Waxman, S.G. (2005). Electrophysiological properties of two axonal sodium channels, Nav1.2 and Nav1.6, expressed in mouse spinal sensory neurones. *J. Physiol.* 564, 803–815. <https://doi.org/10.1113/jphysiol.2005.083089>.
 6. Gazina, E.V., Leaw, B.T.W., Richards, K.L., Wimmer, V.C., Kim, T.H., Aumann, T.D., Featherby, T.J., Churilov, L., Hammond, V.E., Reid, C.A., and Petrou, S. (2015). Neonatal Nav1.2 reduces neuronal excitability and affects seizure susceptibility and behaviour. *Hum. Mol. Genet.* 24, 1457–1468. <https://doi.org/10.1093/hmg/ddu562>.
 7. Liang, L., Fazel Darbandi, S., Pochareddy, S., Gulden, F.O., Gilson, M.C., Sheppard, B.K., Sahagun, A., An, J.Y., Werling, D.M., Rubenstein, J.L.R., et al. (2021). Developmental dynamics of voltage-gated sodium channel isoform expression in the human and mouse brain. *Genome Med.* 13, 135. <https://doi.org/10.1186/s13073-021-00949-0>.
 8. Heighway, J., Sedo, A., Garg, A., Eldershaw, L., Perreau, V., Berecki, G., Reid, C.A., Petrou, S., and Maljevic, S. (2022). Sodium channel expression and transcript variation in the developing brain of human, Rhesus monkey, and mouse. *Neurobiol. Dis.* 164, 105622. <https://doi.org/10.1016/j.nbd.2022.105622>.
 9. Sanders, S.J., Campbell, A.J., Cottrell, J.R., Moller, R.S., Wagner, F.F., Auldridge, A.L., Bernier, R.A., Catterall, W.A., Chung, W.K., Empfield, J.R., et al. (2018). Progress in Understanding and Treating SCN2A-Mediated Disorders. *Trends Neurosci.* 41, 442–456. <https://doi.org/10.1016/j.tins.2018.03.011>.
 10. Wolff, M., Brunklaus, A., and Zuberi, S.M. (2019). Phenotypic spectrum and genetics of SCN2A-related disorders, treatment options, and outcomes in epilepsy and beyond. *Epilepsia* 60 (Suppl 3), S59–S67. <https://doi.org/10.1111/epi.14935>.
 11. Wolff, M., Johannesen, K.M., Hedrich, U.B.S., Masnada, S., Rubboli, G., Gardella, E., Lesca, G., Ville, D., Milh, M., Villard, L., et al. (2017). Genetic and phenotypic heterogeneity suggest therapeutic implications in SCN2A-related disorders. *Brain* 140, 1316–1336. <https://doi.org/10.1093/brain/awx054>.
 12. Crawford, K., Xian, J., Helbig, K.L., Galer, P.D., Parthasarathy, S., Lewis-Smith, D., Kaufman, M.C., Fitch, E., Ganesan, S., O'Brien, M., et al. (2021). Computational analysis of 10,860 phenotypic annotations in individuals with SCN2A-related disorders. *Genet. Med.* 23, 1263–1272. <https://doi.org/10.1038/s41436-021-01120-1>.
 13. Ben-Shalom, R., Keeshen, C.M., Berrios, K.N., An, J.Y., Sanders, S.J., and Bender, K.J. (2017). Opposing Effects on Nav1.2 Function Underlie Differences Between SCN2A Variants Observed in Individuals With Autism Spectrum Disorder or Infantile Seizures. *Biol. Psychiatr.* 82, 224–232. <https://doi.org/10.1016/j.biopsych.2017.01.009>.
 14. Berecki, G., Howell, K.B., Deerasooriya, Y.H., Cilio, M.R., Oliva, M.K., Kaplan, D., Scheffer, I.E., Berkovic, S.F., and Petrou, S. (2018). Dynamic action potential clamp predicts functional separation in mild familial and severe de novo forms of SCN2A epilepsy. *Proc. Natl. Acad. Sci. USA* 115, E5516–E5525. <https://doi.org/10.1073/pnas.1800077115>.
 15. Berecki, G., Howell, K.B., Heighway, J., Olivier, N., Rodda, J., Overmars, I., Vlaskamp, D.R.M., Ware, T.L., Arden-Holmes, S., Lesca, G., et al. (2022). Functional correlates of clinical phenotype and severity in recurrent SCN2A variants. *Commun. Biol.* 5, 515. <https://doi.org/10.1038/s42003-022-03454-1>.
 16. Asadollahi, R., Delvendahl, I., Muff, R., Tan, G., Rodriguez, D.G., Turan, S., Russo, M., Oneda, B., Joset, P., Boonsawat, P., et al. (2023). Pathogenic SCN2A variants cause early-stage dysfunction in patient-derived neurons. *Hum. Mol. Genet.* 32, 2192–2204. <https://doi.org/10.1093/hmg/ddad048>.
 17. Planells-Cases, R., Caprini, M., Zhang, J., Rockenstein, E.M., Rivera, R.R., Murre, C., Masliah, E., and Montal, M. (2000). Neuronal death and perinatal lethality in voltage-gated sodium channel alpha(I)-deficient mice. *Biophys. J.* 78, 2878–2891. [https://doi.org/10.1016/S0006-3495\(00\)76829-9](https://doi.org/10.1016/S0006-3495(00)76829-9).
 18. Shin, W., Kweon, H., Kang, R., Kim, D., Kim, K., Kang, M., Kim, S.Y., Hwang, S.N., Kim, J.Y., Yang, E., et al. (2019). Scn2a Haploinsufficiency in Mice Suppresses Hippocampal Neuronal Excitability, Excitatory Synaptic Drive, and Long-Term Potentiation, and Spatial Learning and Memory. *Front. Mol. Neurosci.* 12, 145. <https://doi.org/10.3389/fnmol.2019.00145>.
 19. Tatsukawa, T., Raveau, M., Ogiwara, I., Hattori, S., Miyamoto, H., Mazaki, E., Itohara, S., Miyakawa, T., Montal, M., and Yamakawa, K. (2019). Scn2a haploinsufficient mice display a spectrum of phenotypes affecting anxiety, sociability, memory flexibility and ampakine CX516 rescues their hyperactivity. *Mol. Autism* 10, 15. <https://doi.org/10.1186/s13229-019-0265-5>.
 20. Léna, I., and Mantegazza, M. (2019). Nav1.2 haploinsufficiency in Scn2a knock-out mice causes an autistic-like phenotype attenuated with age. *Sci. Rep.* 9, 12886. <https://doi.org/10.1038/s41598-019-49392-7>.
 21. Zhang, J., Chen, X., Eaton, M., Wu, J., Ma, Z., Lai, S., Park, A., Ahmad, T.S., Que, Z., Lee, J.H., et al. (2021). Severe deficiency of the voltage-gated sodium channel Nav1.2 elevates neuronal excitability in adult mice. *Cell Rep.* 36, 109495. <https://doi.org/10.1016/j.celrep.2021.109495>.
 22. Spratt, P.W.E., Alexander, R.P.D., Ben-Shalom, R., Sahagun, A., Kyoung, H., Keeshen, C.M., Sanders, S.J., and Bender, K.J. (2021). Paradoxical hyperexcitability from Nav1.2 sodium channel loss in neocortical pyramidal cells. *Cell Rep.* 36, 109483. <https://doi.org/10.1016/j.celrep.2021.109483>.
 23. Ma, Z., Eaton, M., Liu, Y., Zhang, J., Chen, X., Tu, X., Shi, Y., Que, Z., Wetttschurack, K., Zhang, Z., et al. (2022). Deficiency of autism-related Scn2a gene in mice disrupts sleep patterns and circadian rhythms. *Neurobiol. Dis.* 168, 105690. <https://doi.org/10.1016/j.nbd.2022.105690>.
 24. Waters, J., Schaefer, A., and Sakmann, B. (2005). Backpropagating action potentials in neurones: measurement, mechanisms and potential functions. *Prog. Biophys. Mol. Biol.* 87, 145–170. <https://doi.org/10.1016/j.pbiomolbio.2004.06.009>.
 25. Stuart, G., Spruston, N., Sakmann, B., and Häusser, M. (1997). Action potential initiation and backpropagation in neurons of the mammalian CNS. *Trends Neurosci.* 20, 125–131. [https://doi.org/10.1016/s0166-2236\(96\)10075-8](https://doi.org/10.1016/s0166-2236(96)10075-8).
 26. Larkum, M.E., Senn, W., and Lüscher, H.R. (2004). Top-down dendritic input increases the gain of layer 5 pyramidal neurons. *Cereb. Cortex* 14, 1059–1070. <https://doi.org/10.1093/cercor/bbh065>.
 27. Larkum, M.E., Zhu, J.J., and Sakmann, B. (1999). A new cellular mechanism for coupling inputs arriving at different cortical layers. *Nature* 398, 338–341. <https://doi.org/10.1038/18686>.
 28. Balasco, L., Provenzano, G., and Bozzi, Y. (2019). Sensory Abnormalities in Autism Spectrum Disorders: A Focus on the Tactile Domain, From Genetic Mouse Models to the Clinic. *Front. Psychiatr.* 10, 1016. <https://doi.org/10.3389/fpsy.2019.01016>.
 29. Antoine, M.W., Langberg, T., Schnepel, P., and Feldman, D.E. (2019). Increased Excitation-Inhibition Ratio Stabilizes Synapse and Circuit Excitability in Four Autism Mouse Models. *Neuron* 101, 648–661.e4. <https://doi.org/10.1016/j.neuron.2018.12.026>.
 30. Li, M., Jancovski, N., Jafar-Nejad, P., Burbano, L.E., Rollo, B., Richards, K., Drew, L., Sedo, A., Heighway, J., Pachernegg, S., et al. (2021). Antisense oligonucleotide therapy reduces seizures and extends life span in an SCN2A gain-of-function epilepsy model. *J. Clin. Invest.* 131, e152079. <https://doi.org/10.1172/JCI152079>.
 31. DeVos, S.L., and Miller, T.M. (2013). Direct intraventricular delivery of drugs to the rodent central nervous system. *J. Vis. Exp.* e50326. <https://doi.org/10.3791/50326>.
 32. Jafar-Nejad, P., Powers, B., Soriano, A., Zhao, H., Norris, D.A., Matson, J., DeBrosse-Serra, B., Watson, J., Narayanan, P., Chun, S.J., et al. (2021). The atlas of RNase H antisense oligonucleotide distribution and activity in the CNS of rodents and non-human primates following central administration. *Nucleic Acids Res.* 49, 657–673. <https://doi.org/10.1093/nar/gkaa1235>.
 33. Rigo, F., Chun, S.J., Norris, D.A., Hung, G., Lee, S., Matson, J., Fey, R.A., Gaus, H., Hua, Y., Grundy, J.S., et al. (2014). Pharmacology of a central nervous system delivered 2'-O-methoxyethyl-modified survival of motor neuron splicing oligonucleotide in mice and nonhuman primates. *J. Pharmacol. Exp. Therapeut.* 350, 46–55. <https://doi.org/10.1124/jpet.113.212407>.
 34. Eaton, M., Zhang, J., Ma, Z., Park, A.C., Lietzke, E., Romero, C.M., Liu, Y., Coleman, E.R., Chen, X., Xiao, T., et al. (2021). Generation and basic characterization of a gene-trap knockout mouse model of Scn2a with a substantial reduction of voltage-gated sodium channel Nav 1.2 expression. *Gene Brain Behav.* 20, e12725. <https://doi.org/10.1111/gbb.12725>.
 35. Miyamoto, H., Tatsukawa, T., Shimohata, A., Yamagata, T., Suzuki, T., Amano, K., Mazaki, E., Raveau, M., Ogiwara, I., Oba-Asaka, A., et al. (2019). Impaired cortico-striatal excitatory transmission triggers epilepsy. *Nat. Commun.* 10, 1917. <https://doi.org/10.1038/s41467-019-09954-9>.
 36. Ogiwara, I., Miyamoto, H., Tatsukawa, T., Yamagata, T., Nakayama, T., Atapour, N., Miura, E., Mazaki, E., Ernst, S.J., Cao, D., et al. (2018). Nav1.2 haploinsufficiency in excitatory neurons causes absence-like seizures in mice. *Commun. Biol.* 1, 96. <https://doi.org/10.1038/s42003-018-0099-2>.

37. Middleton, S.J., Kneller, E.M., Chen, S., Ogiwara, I., Montal, M., Yamakawa, K., and McHugh, T.J. (2018). Altered hippocampal replay is associated with memory impairment in mice heterozygous for the *Scn2a* gene. *Nat. Neurosci.* 21, 996–1003. <https://doi.org/10.1038/s41593-018-0163-8>.
38. Yu, Z., Guindani, M., Grieco, S.F., Chen, L., Holmes, T.C., and Xu, X. (2022). Beyond t test and ANOVA: applications of mixed-effects models for more rigorous statistical analysis in neuroscience research. *Neuron* 110, 21–35. <https://doi.org/10.1016/j.neuron.2021.10.030>.
39. Hamm, J.P., Peterka, D.S., Gogos, J.A., and Yuste, R. (2017). Altered Cortical Ensembles in Mouse Models of Schizophrenia. *Neuron* 94, 153–167.e8.e158. <https://doi.org/10.1016/j.neuron.2017.03.019>.
40. Cossart, R., Aronov, D., and Yuste, R. (2003). Attractor dynamics of network UP states in the neocortex. *Nature* 423, 283–288. <https://doi.org/10.1038/nature01614>.
41. Dhir, A. (2012). Chapter. Pentylentetrazol (PTZ) kindling model of epilepsy. *Curr. Protoc. Neurosci. Chapter 9, Unit9.37*. <https://doi.org/10.1002/0471142301.ns0937s58>.
42. da Silva, L.F., Pereira, P., and Elisabetsky, E. (1998). A neuropharmacological analysis of PTZ-induced kindling in mice. *Gen. Pharmacol.* 31, 47–50. [https://doi.org/10.1016/s0306-3623\(97\)00423-0](https://doi.org/10.1016/s0306-3623(97)00423-0).
43. Augustinaite, S., and Kuhn, B. (2020). Complementary Ca(2+) Activity of Sensory Activated and Suppressed Layer 6 Corticothalamic Neurons Reflects Behavioral State. *Curr. Biol.* 30, 3945–3960.e5. <https://doi.org/10.1016/j.cub.2020.07.069>.
44. Depreux, F.F., Wang, L., Jiang, H., Jodelka, F.M., Rosencrans, R.F., Rigo, F., Lentz, J.J., Brigande, J.V., and Hastings, M.L. (2016). Antisense oligonucleotides delivered to the amniotic cavity in utero modulate gene expression in the postnatal mouse. *Nucleic Acids Res.* 44, 9519–9529. <https://doi.org/10.1093/nar/gkw867>.
45. Funamizu, A., Kuhn, B., and Doya, K. (2016). Neural substrate of dynamic Bayesian inference in the cerebral cortex. *Nat. Neurosci.* 19, 1682–1689. <https://doi.org/10.1038/nn.4390>.
46. Helmchen, F., and Denk, W. (2005). Deep tissue two-photon microscopy. *Nat. Methods* 2, 932–940. <https://doi.org/10.1038/nmeth818>.
47. Chen, T.W., Wardill, T.J., Sun, Y., Pulver, S.R., Renninger, S.L., Baohan, A., Schreiter, E.R., Kerr, R.A., Orger, M.B., Jayaraman, V., et al. (2013). Ultrasensitive fluorescent proteins for imaging neuronal activity. *Nature* 499, 295–300. <https://doi.org/10.1038/nature12354>.
48. Wang, H.G., Bavley, C.C., Li, A., Jones, R.M., Hackett, J., Bayley, Y., Lee, F.S., Rajadhyaksha, A.M., and Pitt, G.S. (2021). *Scn2a* severe hypomorphic mutation decreases excitatory synaptic input and causes autism-associated behaviors. *JCI Insight* 6, e150698. <https://doi.org/10.1172/jci.insight.150698>.
49. Kim, S., Kim, Y.E., Song, I., Ujihara, Y., Kim, N., Jiang, Y.H., Yin, H.H., Lee, T.H., and Kim, I.H. (2022). Neural circuit pathology driven by *Shank3* mutation disrupts social behaviors. *Cell Rep.* 39, 110906. <https://doi.org/10.1016/j.celrep.2022.110906>.
50. Michaelson, S.D., Ozkan, E.D., Aceti, M., Maity, S., Llamas, N., Weldon, M., Mizrahi, E., Vaissiere, T., Gaffield, M.A., Christie, J.M., et al. (2018). SYNGAP1 heterozygosity disrupts sensory processing by reducing touch-related activity within somatosensory cortex circuits. *Nat. Neurosci.* 21, 1–13. <https://doi.org/10.1038/s41593-018-0268-0>.
51. Meredith, R.M., Holmgren, C.D., Weidum, M., Burnashev, N., and Mansvelder, H.D. (2007). Increased threshold for spike-timing-dependent plasticity is caused by unreliable calcium signaling in mice lacking fragile X gene *FMR1*. *Neuron* 54, 627–638. <https://doi.org/10.1016/j.neuron.2007.04.028>.
52. Gunaydin, L.A., Grosenick, L., Finkelstein, J.C., Kauvar, I.V., Fenno, L.E., Adhikari, A., Lammel, S., Mirzabekov, J.J., Airan, R.D., Zalocusky, K.A., et al. (2014). Natural neural projection dynamics underlying social behavior. *Cell* 157, 1535–1551. <https://doi.org/10.1016/j.cell.2014.05.017>.
53. Murugan, M., Jang, H.J., Park, M., Miller, E.M., Cox, J., Taliaferro, J.P., Parker, N.F., Bhawe, V., Hur, H., Liang, Y., et al. (2017). Combined Social and Spatial Coding in a Descending Projection from the Prefrontal Cortex. *Cell* 171, 1663–1677.e16. <https://doi.org/10.1016/j.cell.2017.11.002>.
54. Liang, B., Zhang, L., Barbera, G., Fang, W., Zhang, J., Chen, X., Chen, R., Li, Y., and Lin, D.T. (2018). Distinct and Dynamic ON and OFF Neural Ensembles in the Prefrontal Cortex Code Social Exploration. *Neuron* 100, 700–714.e9.e709. <https://doi.org/10.1016/j.neuron.2018.08.043>.
55. Fallah, M.S., and Eubanks, J.H. (2020). Seizures in Mouse Models of Rare Neurodevelopmental Disorders. *Neuroscience* 445, 50–68. <https://doi.org/10.1016/j.neuroscience.2020.01.041>.
56. Burbano, L.E., Li, M., Jancovski, N., Jafar-Nejad, P., Richards, K., Sedo, A., Soriano, A., Rollo, B., Jia, L., Gazina, E.V., et al. (2022). Antisense oligonucleotide therapy for KCNT1 encephalopathy. *JCI Insight* 7, e146090. <https://doi.org/10.1172/jci.insight.146090>.
57. Kuhn, B., and Roome, C.J. (2019). Primer to Voltage Imaging With ANNINE Dyes and Two-Photon Microscopy. *Front. Cell. Neurosci.* 13, 321. <https://doi.org/10.3389/fncel.2019.00321>.
58. Roome, C.J., and Kuhn, B. (2018). Simultaneous dendritic voltage and calcium imaging and somatic recording from Purkinje neurons in awake mice. *Nat. Commun.* 9, 3388. <https://doi.org/10.1038/s41467-018-05900-3>.
59. Sacai, H., Sakoori, K., Konno, K., Nagahama, K., Suzuki, H., Watanabe, T., Watanabe, M., Uesaka, N., and Kano, M. (2020). Autism spectrum disorder-like behavior caused by reduced excitatory synaptic transmission in pyramidal neurons of mouse prefrontal cortex. *Nat. Commun.* 11, 5140. <https://doi.org/10.1038/s41467-020-18861-3>.
60. Luo, Y.F., Lu, L., Song, H.Y., Xu, H., Zheng, Z.W., Wu, Z.Y., Jiang, C.C., Tong, C., Yuan, H.Y., Liu, X.X., et al. (2023). Divergent projections of the prelimbic cortex mediate autism- and anxiety-like behaviors. *Mol. Psychiatr.* <https://doi.org/10.1038/s41380-023-01954-y>.
61. Glickfeld, L.L., Andermann, M.L., Bonin, V., and Reid, R.C. (2013). Cortico-cortical projections in mouse visual cortex are functionally target specific. *Nat. Neurosci.* 16, 219–226. <https://doi.org/10.1038/nn.3300>.
62. Kozorovitskiy, Y., Saunders, A., Johnson, C.A., Lowell, B.B., and Sabatini, B.L. (2012). Recurrent network activity drives striatal synaptogenesis. *Nature* 485, 646–650. <https://doi.org/10.1038/nature11052>.
63. Gerfen, C.R., Paletzki, R., and Heintz, N. (2013). GENSAT BAC cre-recombinase driver lines to study the functional organization of cerebral cortical and basal ganglia circuits. *Neuron* 80, 1368–1383. <https://doi.org/10.1016/j.neuron.2013.10.016>.
64. Augustinaite, S., and Kuhn, B. (2020). Chronic Cranial Window for Imaging Cortical Activity in Head-Fixed Mice. *STAR Protoc.* 1, 100194. <https://doi.org/10.1016/j.xpro.2020.100194>.
65. Deacon, R.M.J. (2006). Assessing nest building in mice. *Nat. Protoc.* 1, 1117–1119. <https://doi.org/10.1038/nprot.2006.170>.
66. Pnevmatikakis, E.A., and Giovannucci, A. (2017). NoRMCorre: An online algorithm for piecewise rigid motion correction of calcium imaging data. *J. Neurosci. Methods* 291, 83–94. <https://doi.org/10.1016/j.jneumeth.2017.07.031>.
67. Flotho, P., Nomura, S., Kuhn, B., and Strauss, D.J. (2022). Software for Non-Parametric Image Registration of 2-Photon Imaging Data. *J. Biophot.* 15, e202100330. <https://doi.org/10.1002/jbio.202100330>.
68. Giovannucci, A., Friedrich, J., Gunn, P., Kalfon, J., Brown, B.L., Koay, S.A., Taxis, J., Najafi, F., Gauthier, J.L., Zhou, P., et al. (2019). CalmAn an open source tool for scalable calcium imaging data analysis. *Elife* 8, e38173. <https://doi.org/10.7554/eLife.38173>.
69. Tadel, F., Baillet, S., Mosher, J.C., Pantazis, D., and Leahy, R.M. (2011). Brainstorm: a user-friendly application for MEG/EEG analysis. *Comput. Intell. Neurosci.* 2011, 879716. <https://doi.org/10.1155/2011/879716>.

STAR★METHODS

KEY RESOURCES TABLE

REAGENT or RESOURCE	SOURCE	IDENTIFIER
Experimental models: Organisms/strains		
Rbp4-Cre mice	Mutant Mouse Resource & Research Centers	037128-UCD
Bacterial and virus strains		
AAV1.Syn.Flex.GCaMP6f.WPRE.SV40	Addgene	100833-AAV1
Oligonucleotides		
Scn2a ASO	IDT, Japan	Please see sequence in Methods Details
Chemicals, peptides, and recombinant proteins		
Pentylentetrazol	Biosynth	FP26833
Mg ²⁺ , Ca ²⁺ free phosphate-buffered saline	Thermo Fisher Scientific	10010031
Antibodies		
Anti-Nav1.2 antibodies	Alomone Labs	Cat# ASC-002; RRID: AB_2040005
Anti-Gapdh antibodies	Millipore	Cat# MAB374; RRID:AB_2107445
Software and algorithms		
Customized MATLAB script	Mathworks	https://mathworks.com
ImageJ	NIH	https://ImageJ.net/ij/index.html
Brainstorm	Brainstorm	http://neuroimage.usc.edu/brainstorm
Graphpad Prism 9	GraphPad, Dotmatics	https://www.graphpad.com/
Deposited data		
All dataset and analysis scripts are available on Dryad	Dryad	https://doi.org/10.5061/dryad.83bk3j9z2

RESOURCE AVAILABILITY

Lead contact

- All data have been deposited at Dryad and are publicly available as of the date of publication. DOIs are listed in the [key resources table](#).
- All original code has been deposited at Dryad and is publicly available as of the date of publication. DOIs are listed in the [key resources table](#).
- Any additional information required to reanalyze the data reported in this paper is available from the [lead contact](#) upon request, bkuhn@oist.jp (Bernd Kuhn).

Materials availability

This study did not generate new unique reagents.

Data and code availability

- All data reported in this paper will be shared by the [lead contact](#) upon request.
- All datasets and analysis scripts are deposited to Dryad.

EXPERIMENTAL MODEL AND STUDY PARTICIPANT DETAILS

Animals

Animal experiments were in accordance with the Institutional Animal Care and Use Committees of the Okinawa Institute of Science and Technology Graduate University (OIST). Procedures were performed in an Association for Assessment and Accreditation of Laboratory Animal Care (AAALAC International) accredited facility. The Cre-recombinase bacterial artificial chromosome transgenic mouse line, Rbp4-Cre mouse model, was obtained from the Mutant Mouse Resource & Research Centers (MMRRC). The Rbp4-Cre mouse line enables

selective labeling of predominantly L5 pyramidal neurons.^{61–63} Genotype was determined by polymerase chain reaction (PCR) with primers (5' to 3'): Forward GGGCGGCCTCGGTCTC; Reverse CCCAGAAATGCCAGATTACGTAT. The colony was maintained by back-crossing hemizygous males with C57/Bl6J females. Male Rbp4-Cre mice aged between 2 and 3 months were used for experiments. Animals were housed in a temperature-controlled room (22°C) with a 12-h reversed light on/off cycle, and free access to food and water.

METHOD DETAILS

Drug preparation

The ASO downregulating mouse Scn2a mRNA (Scn2a ASO) was commercially synthesized (IDT Japan). The Scn2a ASO sequence, chemical modifications and selectivity were detailed in a previous study.³⁰ The Scn2a ASO nucleotide sequence was GCTCATGTTACTCCTACCCT with 5 MOE-modified nucleotides at each end of the oligonucleotide, and 10 DNA nucleotides in the center. The Scn2a ASO was reconstituted in sterile Ca²⁺ and Mg²⁺ free phosphate buffer saline (PBS, Gibco) and stored at 4°C. Pentylentetrazol (PTZ, Biosynth) was stored at –20°C. Working aliquot was made in 0.9% saline just before use. PTZ (50 mg/kg, s.c., 10 mL/kg) was administered into the animal during experiment. This PTZ dose is known to induce epileptiform activities on the ECoG without causing overt convulsion.^{41,42}

Quantitative gene expression analysis (RT-qPCR)

Four weeks after intracerebroventricular (ICV) injection, mice were deeply anesthetized with isoflurane until no hindlimb and corneal reflex was observed. The cerebral hemisphere was collected, immediately snap-frozen in liquid nitrogen and stored at –80°C until analysis. RNA extraction and RT-qPCR were performed by Macrogen Japan. RNA was extracted using Trizol reagent as per manufacturer's instructions (Invitrogen), followed by DNase I treatment. RNA quality was determined using Agilent Technologies 2100 Bioanalyzer. Samples with RNA Integrity Number value ≥ 7.5 were proceeded to RT-qPCR.

cDNA was produced using the Superscript RT-PCR System (Invitrogen) according to the manufacture's guideline for oligo(dT)20 primed cDNA-synthesis. cDNA synthesis was performed on 500 ng of RNA at 42°C then diluted by a ratio of 1:2. The Taqman probes targeting mouse VGSC isoforms used in this study were as follow: Scn1a (GenBank: Mm00450580_m1), Scn2a (GenBank: Mm01270367_m1), and Scn8a (GenBank: Mm00488123_m1). The mouse Gapdh gene was used as control probe (Genbank: Hs99999905_m1). RT-qPCR was performed in an ABI PRISM 7900HT Sequence Detection System (Applied Biosystems). All samples were amplified on triplicate and data were analyzed with Sequence Detector software (Applied Biosystems). Relative gene abundance values were calculated by normalization to Gapdh and referenced to the control group (PBS) using the $2^{-\Delta\Delta C_t}$ method.

Western blotting

Four weeks after ICV injection, mice were deeply anesthetized with isoflurane until no hindlimb and corneal reflex was observed. The cerebral hemisphere was collected, immediately snap-frozen in liquid nitrogen and stored at –80°C until analysis. Brain homogenates were prepared by plastic homogenizer in RIPA buffer (Nacalai, cat# 16488-34) containing 50 mmol/L Tris-HCl Buffer (pH 7.6), 150 mmol/L NaCl, 1% Nonidet P-40 Substitute, 0.5% sodium deoxycholate, 0.1% SDS with protease inhibitor added (Abcam, cat# ab141032) and kept in 4°C for 30 min. The lysates were centrifuged at 21,000 rpm for 30 min and supernatants were collected as protein samples. Protein concentrations were measured and quantified using Bradford assay based on known BSA standard series. 40 μ g of each sample were separated on 4–15% Mini-PROTEAN TGX Precast Protein Gels (Biorad, cat# 4561084) and transferred to PVDF membrane using Invitrogen iBlot 2 Gel Transfer Device (Invitrogen). The membrane was immunoblotted with anti-NaV1.2 sodium channel (1:500, Alomone Labs, Cat# ASC-002), and anti-Gapdh (1:5000; Millipore, Cat# MAB374) antibodies. The blots were visualized by chemiluminescence, and images were captured using iBright 1500 Imaging System (Invitrogen) and quantified using ImageJ.

Surgery

Mice (2–3 months old) were deeply anesthetized with a mixture of medetomidine (0.3 mg/kg), midazolam (4 mg/kg) and butorphanol (5 mg/kg). A craniotomy was performed by thinning and removal of skull over SCx, diameter was approximately 5 mm.⁶⁴ Following craniotomy, the adeno-associated virus serotype 1 driving Cre-dependent expression of GCaMP6f (AAV1.Syn.Flex.GCaMP6f.WPRE.SV40 was a gift from Douglas Kim & GENIE Project, Addgene, 100833-AAV1, titer 1.9×10^{13} GC/mL) were injected into L5 of the primary somatosensory cortex (S1 Cx) over 3–5 min. The virus injection co-ordinates were (from bregma): AP -1 mm, ML 2.5 mm, DV 0.75 mm. A chronic cranial window (5 mm diameter glass coverslip) was positioned to enable imaging of S1 Cx. Two silver wires were placed on the dura of S1 Cx for ECoG recording. Because ASO do not cross the blood brain barrier, on the contralateral side of craniotomy, the Scn2a ASO (500 μ g) or the negative control, PBS, were delivered via ICV injection. The Scn2a ASO dose was selected based on previous study and is expected to achieve >90% reduction in Scn2a mRNA.³⁰ The ICV injection co-ordinates were (from bregma): AP +0.3 mm, ML 1 mm, DV 3 mm. ICV injection volume was 5 μ L, at a rate of 0.5 μ L/s. A previous study confirmed the wide-spread distribution of ASO in mouse brain using ICV injection.³⁰

Behavioral tests

Behavioral experiments were performed 2–3 weeks after surgery, during the dark phase between 09:00 and 13:00 h. The same test sequence was performed on 5 independent cohorts of mice (N = 3–7 mice per cohort): open field \rightarrow nesting \rightarrow elevated plus maze \rightarrow three-chamber

social interaction. Mice were acclimatized to the testing rooms for at least 30 min before experimentation and were given minimum overnight recovery in between tests. Equipment was cleaned with 70% ethanol then water between testing of each mouse.

Open field

The mouse was placed in the center of a 40 × 40 cm chamber (O'hara) with lighting at 100 lux. Its position and locomotor activity were tracked by computer software (O'hara) for 15 min. The moving criterion was 3 cm/s. The center region was defined as 36% of the chamber area.

Elevated plus maze

The elevated plus maze (O'hara) contained 2 open arms (25 × 5 cm) and 2 closed arms (25 × 5 cm, enclosed wall height 15 cm) extending from a central platform (5 × 5 cm). The maze is located in a room with a lighting at 100 lux and was elevated 50 cm from the floor. The mouse was placed in the center of the maze at the start of experiment, and its position was tracked by a computer software (O'hara) for 5 min.

Nesting

Mice were individually housed in fresh home cages. Nesting material, which consisted of three pieces of tissues (21 × 12 cm) were placed flatly on the cage floor, opposite of the food tray. Nest quality was assessed 48 h after nesting material was given. A nesting score from 0 to 5 was determined for each mouse, where 5 indicates the highest quality.⁶⁵

Three-chamber social interaction test

The three-chamber apparatus consisted of a rectangular box (40 × 60 cm) partitioned into three compartments. At the start of each trial, mouse was placed in the center compartment (width 10 cm) which contained an opening on the clear wall to allow for free access into each of the two equal sized compartments (width 21 cm). A wired chamber in the shape of quartered circle (radius 10 cm) was placed in the corner of each of the two outside compartments. The stranger mice were placed inside the wired chamber and the interaction zone was defined as 2 cm in front of the wired chamber. Mouse activity was monitored by a camera and analyzed by dedicated computer software (O'hara).

The test consists of three consecutive trials, each lasting 10 min. In the first trial, both wired chambers were empty. In the second trial, an unfamiliar, age-, strain-, and sex-matched stranger mouse was placed in the right wired chamber while the left wired chamber remained empty. In the last trial, another unfamiliar, age-, strain-, and sex-matched stranger mouse was placed in the left wired chamber. The mouse in the right wired chamber remained in the same position and now became the familiar mouse. The test was performed at a lighting of 10 lux.

Simultaneous *in vivo* Ca²⁺ imaging and electrocorticography

Imaging experiments were performed 3–4 weeks post-surgery. Prior to recording, mice were habituated to head-fixing and the vertically rotating treadmill for minimum five days (each session was 30–45 min). Mice were further habituated to the experimental set up for minimum 30 min before experiments began.

In vivo imaging was performed on a custom-built combined wide-field, two-photon microscope with resonant scanner (MOM, Sutter Instruments). A 25x/N.A. 1.05 water immersion objective (Olympus) with 2 mm working distance was used. The collar of the objective was adjusted to correct for the cranial window thickness (0.17 mm). Bright field imaging was performed using a Nikon camera (D810A). For two-photon imaging, a femtosecond-pulsed Ti:sapphire laser (Vision II, Coherent) was used to excite fluorescence. The excitation wavelength was 950 nm. Fluorescence was detected by a GaAsP photomultiplier (Hamamatsu) within a spectral window of 490–550 nm. Imaging movies were acquired with 512 × 512 pixel per frame, which corresponded to a field of view of 375 × 375 μm. 30.9 frames per second were acquired. The animal was head fixed and was free to move on the treadmill during *in vivo* imaging. A 30-min baseline period was obtained. The pro-convulsant, PTZ (50 mg/kg, s.c.) was then injected, followed by another 30 min of *in vivo* imaging. An amplifier for ECoG (Sigmann Elektronik) was mounted on the platform and connected to the two silver wires implanted during surgery to monitor for seizure related activities after PTZ administration. The ECoG signal was sampled at 1 kHz with band-pass filter between 0.25 and 200 Hz. The acquisition of imaging and ECoG data, as well as the video monitoring of mouse behavior and treadmill rotary motion, were performed by a commercial software (MScan, Sutter Instruments).

In vivo Ca²⁺ imaging and electrocorticography analyses

For Ca²⁺ imaging data, motion artifacts were first corrected by using the non-rigid motion correction algorithm, NoRMCorre, with grid size of 48 × 48.⁶⁶ This was followed by an optical flow-based image registration approach, Flow Registration.⁶⁷ In Flow Registration, images underwent 50 iterations, buffer size was 100 and alpha value was 1.5. A customized MATLAB script based on CalmAn⁶⁸ was used to extract ROI, register fluorescence activity and calculate ΔF/F. Traces were baseline adjusted using 15 percentile function and temporally smoothed by a moving mean of 10 frames. A Butterworth low-pass bidirectional filter (cut-off at 6 Hz) was then applied. For each neuron, Ca²⁺ events were defined as peaks exceeding a threshold of 2.5 standard deviation above ΔF/F baseline.

For single neuron analysis, the Ca²⁺ events were quantified by the following parameters: mean amplitude, frequency (number of Ca²⁺ events per second), mean amplitude (mean amplitude of all Ca²⁺ events) and normalized integral (sum of trace normalized by recording duration).

For pairwise coactivity analysis, a similarity index (SI) of each neuronal pair (A, B) was calculated as the normalized inner product: $SI = \frac{A \cdot B}{\|A\| \|B\|}$. To determine significant similarity, a bootstrapping procedure was performed.⁴⁰ Briefly, each individual neuron time course was shifted randomly in time while maintaining a constant activity level. This shuffling was repeated 500 times to generate a distribution of SI expected at chance level. Observed SI for each neuronal pair was then compared to the surrogate dataset and was determined as significant when passed the 95 percentile otherwise the SI was deemed 0.

ECoG data was analyzed using Brainstorm.⁶⁹ PTZ induced spikes on ECoG were determined when amplitude threshold was five times above standard deviation and duration was less than 80 msec. A customized MATLAB script was used to convert the rotary encoder signal to velocity. Kmeans clustering was then used to determine the running or resting state.

QUANTIFICATION AND STATISTICAL ANALYSIS

For *in vivo* Ca²⁺ imaging data, ICC was first performed to determine if there was high clustering within the neuronal population examined in each experimental animal (Table S1). The equation used was ICC = between animal variance/(between animal variance + within animal variance).

To assess the individual and combined effects of the "Scn2a ASO" (control and Scn2a ASO mice) and "PTZ treatment" (baselines and after PTZ) on different parameters of *in vivo* Ca²⁺ imaging data (Ca²⁺ transient frequency, mean amplitude, normalized integral and pairwise coactivity), a LME model was used. The advantage of the LME model is that it accounts for correlation and dependency among neurons within an animal.³⁸ A MATLAB "fitlme" function with restricted maximum likelihood method was chosen to estimate model parameters. In the LME model formula (Equation1), "Scn2a ASO", "PTZ treatment", and their interaction were considered fixed effects. The random effects were modeled as random intercept for each animal. Within each animal, a random slope was used to account for the dependence among neurons within each animal.

$$y(\text{response variable}) = 1 + \text{Scn2a ASO} * \text{PTZ treatment} + (1 + \text{neuronID}|\text{animalID}) \quad (\text{Equation1})$$

The confidence interval and significance of fixed effect estimates, and their interaction is reported in Table S2. The intercept term of fixed effect coefficients estimates the mean outcome value when all predictors are at baseline (i.e., baseline of control mice). The coefficient for each fixed effect estimates the change of this mean outcome.

For the molecular, behavioral and ECoG data, t-test and, one/two-way ANOVA were performed on Graphpad Prism 9 as stated. Statistical significance was determined when $p < 0.05$ and data were reported in mean \pm s.e.m.